Environ. Sci. Technol. **2005**, *39,* 6162−6169

Reoxidation of Bioreduced Uranium under Reducing Conditions

JIAMIN WAN,*,† TETSU K. TOKUNAGA,† EOIN BRODIE,‡ ZHEMING WANG,§ ZUOPING ZHENG,† DON HERMAN,‡ TERRY C. HAZEN,† MARY K. FIRESTONE,‡ AND STEPHEN R. SUTTON||

Lawrence Berkeley National Laboratory, Berkeley, California 94720, University of California, Berkeley, California 94720, Pacific Northwest National Laboratory, Richland, Washington 99352, and University of Chicago, Chicago, Illinois 60637

Nuclear weapons and fuel production have left many soils and sediments contaminated with toxic levels of uranium (U). Although previous short-term experiments on microbially mediated U(VI) reduction have supported the prospect of immobilizing the toxic metal through formation of insoluble U(IV) minerals, our longer-term (17 months) laboratory study showed that microbial reduction of U can be transient, even under sustained reducing conditions. Uranium was reduced during the first 80 days, but later (100−500 days) reoxidized and solubilized, even though a microbial community capable of reducing U(VI) was sustained. Microbial respiration caused increases in (bi)-carbonate concentrations and formation of very stable uranyl carbonate complexes, thereby increasing the thermodynamic favorability of U(IV) oxidation. We propose that kinetic limitations including restricted mass transfer allowed Fe-(III) and possibly Mn(IV) to persist as terminal electron acceptors (TEAs) for U reoxidation. These results show that in-situ U remediation by organic carbon-based reductive precipitation can be problematic in sediments and groundwaters with neutral to alkaline pH, where uranyl carbonates are most stable.

Introduction

Interest in understanding the biogeochemical cycle of uranium and other actinides continues to grow, especially recently for remediating environments contaminated during the course of uranium mining, and production of nuclear fuel and weapons. The U.S. Department of Energy (DOE) alone has an environmental legacy that includes 6 billion m^3 of contaminated groundwater in 5700 distinct plumes, 40 million m^3 of contaminated sediments and debris, and 3 million m^3 of waste buried in landfills, trenches, and spill areas (*1*). The mobility of uranium depends strongly on its oxidation state, with U(IV) species being much less soluble than U(VI) species under most environmental conditions (*2*). Based on findings that a number of Fe- and S-reducing bacteria also reduce U(VI) enzymatically as well as indirectly (*3*−*6*), some strategies under development for immobilizing U(VI) in contaminated sediments and groundwaters are aimed at promoting reductive precipitation of low solubility U(IV) minerals. These emerging techniques rely on injecting organic carbon (OC) into contaminated sediments to stimulate microbial U(VI) reduction to U(IV) solids (e.g., *7*−*9*).

Although reduction-based remediation will require long-term immobilization, observations of OC-stimulated U reduction have only reported results to ∼100 days after conversion to U(IV). Dissolved oxygen, nitrate, and denitrification products have been shown to oxidize U(IV) (*10*−*12*), as expected from simple inspection of the redox ladder. When influxes of highly oxidizing TEAs are prevented, U(IV) is commonly assumed to be permanently stable in reducing sediments. However, this critical assumption underlying in-situ U bioremediation has not previously been tested under controlled, environmentally relevant conditions. Stimulating microbial activity through OC infusion not only lowers pe, but also influences U speciation in other ways. Another major consequence of promoting microbial respiration is that it raises the partial pressure of CO_2 (P_{CO_2}) and concentration of (bi)carbonate. While the P_{CO_2} influence on U(VI) speciation is widely recognized, its influence on U(IV)/U(VI) equilibrium is not. At neutral and alkaline pH, elevated levels of dissolved (bi)carbonate shift U(IV)/U(VI) equilibria to lower redox potentials because strong U(VI)−carbonate complexes are formed (*2*). The possibility that (bi)carbonate accumulation from microbial respiration in the presence of residual TEAs could facilitate solubilization and oxidation of UO_2 appears to have been overlooked in all previous studies of U bioreduction. In this study, columns packed with heavily U-contaminated sediments were infused with sufficient OC to maintain reducing conditions desired for U bioreduction. The long-term (500 days) stability of U reduction was evaluated through measurements of U, OC, and bicarbonate in effluents, and U oxidation states within column sediments. The composition of the sediment microbial community was also assessed to detect relevant changes in the microbial catalysts.

Methods

Sediment Columns. OC solutions were infused through columns of U-contaminated sediments to promote U bioreduction. Columns were made of polycarbonate pipe sections of 200 mm length, 32 mm i.d., and 3.2 mm wall. A narrow window (12 mm by 200 mm, 1.2 mm thick) was milled into one side of each column for in-situ measurements of U oxidation states by synchrotron X-ray absorption spectroscopy. The column outlets permitted continuous collection of effluents into fraction collectors as well as periodic in-line liquid/gas sampling and pH measurements prior to discharge. Historically U-contaminated sediments from "Area 2" of the DOE Natural and Accelerated Bioremediation (NABIR) Program's Field Research Center (FRC) in Oak Ridge National Laboratory, Tennessee, were packed into 12 columns. A wide range of geochemical conditions, including U concentrations, exists in soils and sediments from the FRC (*13*). To ensure reproducibility among these replicate columns, the saturated sediments were extruded through a 5.6 mm sieve to remove the coarsest gravel fraction, then homogenized before packing into the columns. Most of the preparation was performed under a N_2 atmosphere. The composition of the homogenized sediments is described later. The columns were packed with the homogenized sediments to a bulk density of 1.48 Mg m^{-3} (porosity = 0.45). Na-lactate (10.7 mM, 32 mM OC) was added to a simulated groundwater (1 mM NaCl, 1 mM $CaCl_2$, 1 mM $MgCl_2$, 1 mM KCl, pH 7.2). This solution was supplied at an

* Corresponding author phone: (510)486-6004; fax: (510)486-7797; e-mail: jmwan@lbl.gov.
† Lawrence Berkeley National Laboratory.
‡ University of California.
§ Pacific Northwest National Laboratory.
|| University of Chicago.

10.1021/es048236g CCC: $30.25

Published on Web 07/16/2005

average pore fluid velocity of 13 mm d^{-1} for the first 215 days, and thereafter at 10 mm d^{-1}. These flow rates are within the low range of groundwater velocities. To ensure long-term anoxic performance, columns were placed in N_2 purged bags and effluents were collected in a N_2 glovebox. Concentrations of U (kinetic phosphorimetry, KPA, Chemchek), OC and inorganic carbon (TIC-TOC analyzer, O-I Analytical), CH_4 and CO_2 (gas chromatography), Fe, Mn, and Ca (ICP) were measured in effluents. Samples for inorganic carbon and gas analyses were collected in-line into sealed vials (before reaching the fraction collector). pH measurements were obtained both in-line and after the fluids were collected. Five Pt electrodes were embedded along the length of each column for redox measurements. Redox potentials were also calculated on the basis of measured pH and ratios of CH_4 and CO_2 concentrations.

Micro-XANES Spectroscopy. U oxidation states were determined at the Advanced Photon Source, GSECARS beamline 13ID-C, by synchrotron micro-X-ray absorption near edge structure (μ-XANES) spectroscopy (*14*, *15*), for the original sediments and sediment columns. The initial oxidation state distribution was determined on subsamples from the homogenized batch used to pack the columns. The sediment columns were analyzed nondestructively on two separate occasions. Our other experiments have shown that oxygen diffusion through these polycarbonate windows was not detectable for at least as long as 600 days. Because of time constraints, only 3 of the 12 columns were analyzed on both days 107 and 346. μ-XANES spectra were obtained by scanning the entire length of columns in front of the stationary X-ray beam, with monochromatic X-rays scanned through the U L_{III} edge. To rapidly acquire data essential for determining oxidations states at numerous locations within columns, individual locations were scanned at pre-edge, edge, and edge-step energies. Oxidation states of U in the sediments were determined by linear combination fitting of their L_{III} edge energies with those of UO_2 and $UO_2(NO_3)_2{\cdot}6H_2O$, specifically at the half step height energy (*15*).

Fluorescence Spectroscopy. Fluorescence spectroscopic and lifetime measurements (*16*, *17*) were conducted to determine aqueous uranyl species in column effluents. Note that the effluent U concentrations were up to about 1 μM and that reliable extended X-ray absorption fine structure (EXAFS) determination of aqueous uranyl species at such low concentrations is extremely challenging. Fluorescence spectroscopy made the direct determinations of U speciation possible at these low concentrations. The measurements were performed in a CRYO Industries RC152 cryostat at near liquid He-temperature (6 $\pm$ 1 K) using a Spectra-Physics Nd:YAG laser pumped MOPO-730 laser. The emitted light was collected at 85° to the excitation beam. Time-resolved fluorescence spectra were recorded using a thermoelectrically cooled PIMAX intensified CCD camera after dispersion through an Acton SpectroPro 300i double monochromator spectrograph. The U(VI) fluorescence decays were detected by a Hamamatsu R928 photomultiplier tube (PMT) fitted with a Hamamatsu C1392-57 time-gating PMT socket and recorded with a Tektronix TDS 754A digital oscilloscope. Data analysis was performed using the commercial software package IGOR. The three reference compounds used were: (a) uranyl ion: $[UO_2^{2+}] = 5 \times 10^{-5}$ M in nitric acid, pH 2.5; (b) $(UO_2)(CO_3)_3^{4-}$:$[UO_2^{2+}] = 5 \times 10^{-6}$ M in 0.034 M Na_2CO_3, pH = 10.6; (c) $Ca_2UO_2(CO_3)_3$:$[UO_2^{2+}] = 1.17 \times 10^{-4}$ M, $[NaHCO_3] = 7 \times 10^{-3}$ M, $[Ca^{2+}] = 5 \times 10^{-3}$ M, $P_{CO_2} = 10^{-3.5}$ atm, pH = 7.4.

High-Density Oligonucleotide Array Analyses. Microbial communities within sediments were determined using high-density oligonucleotide array analyses on samples from different locations in columns (bottom, middle, and top), and at different stages (U-reduction and U-reoxidation). At each stage, a representative column was destructively sampled and triplicate sediment samples (500 mg) were taken (random samples from homogenized net reduction column material; samples from the column bottom, middle, and top sections from net oxidation columns). DNA was extracted using a BIO101 soil DNA extraction kit (QBiogene, CA) according to the manufacturer's protocol. 16S rDNA PCR was performed in triplicate, and amplicons were pooled for each extract. PCR reactions were performed in a final volume of 100 μL and contained 1x Takara ExTaq PCR buffer, 2 mM $MgCl_2$, 300 nM primers (27F and 1492R) (*18*), 200 μM dNTPs, 50 μg BSA, 0.5 μL of DNA extract and 2.5 U ExTaq DNA polymerase (Takara Mirus Bio Inc., WI), and sterile milliQ H_2O up to 100 μL. Cycling was performed with initial denaturation at 95 °C (5 min) followed by 35 cycles of 95 °C (30 s), 53 °C (30 s), 72 °C (1 min), and a final extension at 72 °C for 7 min. Amplicons were purified using an UltraClean PCR clean up kit (MoBio Inc., CA) according to the manufacturer's protocol and quantified by absorbance at 260 nm.

GeneChips were designed and synthesized as described in De-Santis et al. (*19*). Exactly 2 μg of 16S amplicons was DNaseI fragmented, biotin labeled, and an aliquot (1.85 μg) hybridized to a custom-made Affymetrix GeneChip (Affymetrix, CA) according to the manufacturer's recommended protocol. Hybridization was performed in a rotisserie oven at 60 rpm, 48 °C overnight. GeneChip washing and staining were performed as described previously (*20*). The GeneChip was scanned and recorded as a pixel image and analyzed using standard Affymetrix software (GeneChip Analysis Suite, version 4.0). Signal noise (Q) was calculated as previously described (*20*). Each 25-mer probe has a corresponding mismatch probe whose sequence differs at an internal position (13th base); this enables some detection of non-specific hybridization to reduce false positives. For an individual probe pair to be scored positive, the intensity of fluorescence from the perfectly matched probe (PM) must exceed that of the corresponding mismatch probe (MM) by a factor of 1.15. To be included in the analyses, PM minus MM must exceed 500 times the background noise (500Q). An operational taxonomic unit (OTU) was only considered present if at least 86% of probes for that OTU were positive. This cutoff was determined on the basis of calibration with a 16S rDNA clone library from these sediments (data not shown). The mean difference in intensity between all positive match probes and all corresponding mismatch probes within each probe set for a specific OTU is termed average difference (AD). Changes in AD are indicative of changes in 16S amplicon quantity and can be considered comparable for specific OTUs between samples. However, due to varying probe set hybridization efficiencies, it is not currently possible to determine the relative abundance of different OTUs within a given sample.

Real-Time Quantitative PCR Confirmation of *Geobacteraceae* Population Densities. As targets for DNA array analysis were produced using end-point PCR, quantitative analysis may be subject to bias. For this reason, we used a reliable and more accurate quantitative real-time PCR method to confirm array-observed changes in quantity of *Geobacteraceae*. qPCR was performed using an iCycler iQ real-time detection system (BioRad, CA) with the iQ Sybr Green Supermix (BioRad, CA) kit. Reaction mixtures (final volume, 20 μL) contained 1X iQ Sybr Green Supermix, 6 pmol of each primer, 10 μg pf BSA, 0.5 μL of DNA extract, and DNase/RNase free water. Primers for quantitative real-time PCR (qPCR) were as previously described (*21*). Following enzyme activation (95 °C, 3 min), 40 cycles of 95 °C, 20 s; 51 °C, 20 s; and 72 °C, 30 s were performed. A specific data acquisition step at 85 °C for 10 s was set above the Tm of potential primer dimers to minimize any nonamplicon Sybr Green fluorescence. Copy number of *Geobacteraceae* 16S

TABLE 1. Major Element Composition of Sediment (X-ray Fluorescence) (loi Denotes Loss on Ignition)

	element											
	Na	Mg	Al	Si	P	S	K	Ca	Ti	Mn	Fe	loi
mass %	0.60	1.26	9.51	28.6	0.06	0.01	3.98	1.14	0.45	0.20	4.39	4.63

rDNA molecules was quantified by comparing cycle thresholds to a standard curve (in the range of 10^2-10^8 copies), run in parallel, using *Geobacter* metallireducens GS-15 16S rDNA amplicons generated by PCR using universal bacterial primers 27F and 1492R. Regression coefficients for the standard curves were consistently greater than 0.99, and post amplification melt curve analyses displayed a single peak at 88 °C, indicative of specific *Geobacteraceae* 16S rDNA amplification (data not shown).

Results and Discussion

Characterization of the Original Sediment. Data presented in this section were measured on homogenized sediment after removing large particles (>5.6 mm). This sediment consisted of 30% sand and fine gravel (50 μm−5.6 mm), 41% silt (2−50 μm), and 29% clay (<2 μm). The sediment contained 3.0 mass % of $CaCO_3$ (pressure calcimetry, sediment reacted with 2 N HCl). The pH of the water extract (water:sediment mass ratio = 1:1) was 7.9. The $NO_3^- + NO_2^-$ analyses of the sediment yield 1.1 mg of N (kg sediment)$^{-1}$. Disposal of depleted uranium in this sediment left it with 206 ± 7 mg of U (kg sediment)$^{-1}$ (KPA analyses of acid-digested sediment). The major element composition of the sediment is listed in Table 1.

OC Stimulated U(VI) Reduction and U(IV) Reoxidation. U, OC, and carbonate concentrations (all relative uncertainties < 10%) in effluents from five representative sediment columns are presented in Figure 1. Effluents initially had high U concentrations (Figure 1a), typically exceeding 10 μM, reflecting the originally oxidizing condition. U concentrations decreased rapidly as microbial respiration consumed OC (Figure 1b) and produced (bi)carbonate (Figure 1c) and methane (Table 2). By around day 60, U concentrations declined by 3 orders of magnitude, to less than 30 nM (U.S. EPA drinking water standard for U is 380 nM (*22*)). Thus, in-situ reductive immobilization of U appeared successful at this point and in agreement with many previous studies. Data from in-situ μ-XANES measurements of U oxidation states within sediment columns support this observation (bars in Figure 1a indicate measurement times). Microbes consumed 97% of the lactate, leaving about 1 mM of OC in effluents (Figure 1b). (Bi)carbonate concentrations increased to 15 mM, then decreased to 13 mM after about day 215, coinciding with switching to a lower flow rate (lower rate of OC supply). Increased microbial respiration was also evident from gas bubbles formed in the columns and discharged with effluents. The P_{CO_2} in sediments increased from ~$10^{-3.5}$ to $10^{-1.5}$ atm, and calculated redox potentials dropped down to a pe range of −3.4 to −4.2 (Table 2).

However, beyond about 100 days, increased U concentrations in the effluents were observed in all of the columns, and reached steady state at about 200 days with U concentrations around 1.0 μM. Steady OC consumption (1 mM remained in effluents) and (bi)carbonate (13 mM) and methane (10.4 mM) production indicated that an active microbial population was sustained. The steady high methane production showed that the sediments were reducing. Thus, increases in U concentrations after day 100 occurred under continuously reducing conditions maintained by active microbial populations (described below). Cumulative leaching of U by day 500 still left 97% of the original U in this highly contaminated sediment.

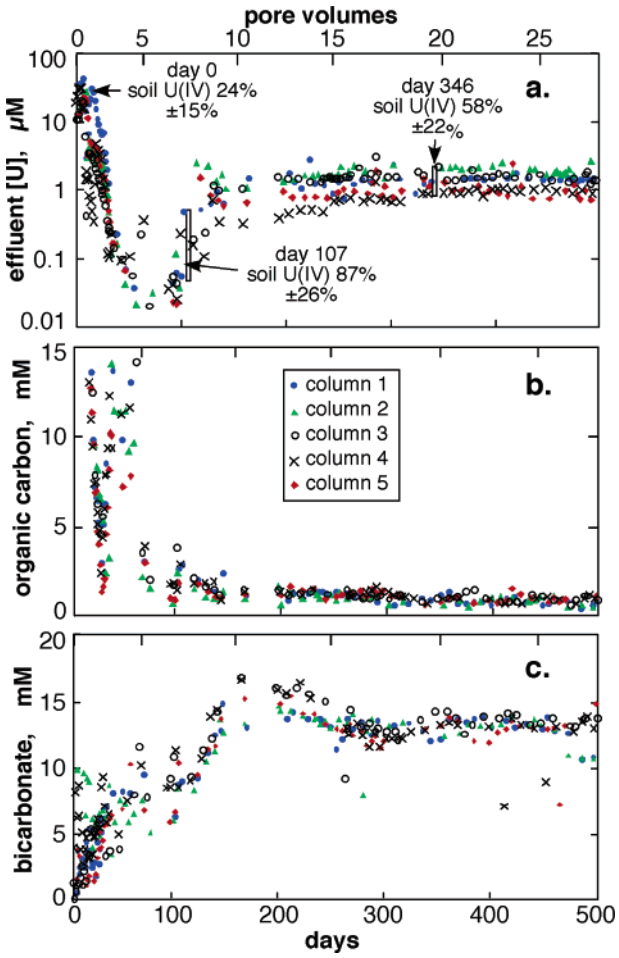

FIGURE 1. U, OC, and bicarbonate concentrations (all relative uncertainties < 10%) from five representative sediment columns. (a) Effluent U concentration trends show declines completed at ~day 60, increases began at ~day 100, and reached steady state at ~day 200. Bars indicate times for μ-XANES measurements of U oxidation states in sediments. (b) OC trends show 97% of injected lactate was being consumed, leaving 1 mM OC in effluents. (c) Bicarbonate trends show this major product of microbial respiration increased to 15 mM, then decreased to 13 mM after about day 215 because of switching to a lower flow rate (lower rate of OC supply).

U Oxidation States. U oxidation states were directly measured on batches of the original sediments, and at two later times within three sediment columns using μ-XANES spectroscopy (Figure 2). Uranium in the original sediment was largely oxidized, with 24 ± 15% occurring as U(IV). Data show variable, but generally reduced, conditions, with 87% (±26%) of the U as U(IV) on day 107. By day 346, the sediment U(IV) declined to 58% (±22%) of the total U. The standard deviations primarily reflect large spatial variability of U(IV) fractions in the sediments at the measurement scale (~1 mm^3 sediment volume, or ~μg sediment mass) rather than valence uncertainty of the spectra (~12%). This variability reflects heterogeneity in chemistry and physical structure at the mm^3 scale resulting from packing columns with up to about 5.6 mm sediment aggregates, and development of nonuniform distributions of flow paths and gas (CO_2 and

TABLE 2. Steady-State Solution Chemistry of Influent and Reoxidation Stage Effluents (Averages and Standard Deviations from 12 Columns)

		influent	steady-state effluent
pH		7.2	7.4 ± 0.14[a]
redox, pe		>0	-3.4 ± 1.0;[b] -4.2 ± 0.3[c]
$\log_{10}$ (P_{CO_2}, atm)		<−3.5	−1.5[d]
OC (lactate)	mM	32.0	1.01 ± 0.25
bicarbonate	mM	0	12.7 ± 1.4
CH_4	mM	0	10.4 ± 1.9
C mass recovery			75%
Ca	mM	1.0	1.5 ± 0.6
Fe	mM	0	0.042 ± 0.008
Mn	mM	0	0.035 ± 0.005
U	μM	0	1.4 ± 0.6

[a] In-situ pH measurements. [b] Measured by using Pt electrodes. [c] Calculated on the basis of measured pH, CO_2, and CH_4 data. [d] Calculated on the basis of measured bicarbonate and pH data.

CH_4) bubbles that are averaged over in more commonly employed bulk (e.g., cm^3) measurements. Despite this variability, the two sets of in-situ μ-XANES analyses were significantly different at $p = 0.005$, demonstrating with greater than 99% confidence that previously bioreduced U(IV) was reoxidized even though strongly reducing conditions were maintained. The overall decrease in the U(IV) fraction despite local variability is evident in 5-point running averages (curves) of individual measurements (points) along μ-XANES profiles taken in the three columns (Figure 2).

The nature of the U(VI) phase was not determined, but several recent studies have reported persistent U(VI) associations with mineral surfaces even under reducing conditions (*23*−*25*). It should also be noted that at the highest measured U(IV) inventory of 87%, a moderately high concentration of U(VI), about 27 mg kg^{-1}, remained in the sediment. Therefore, in addition to the measured net U reoxidation, desorption of unreduced U(VI) and decreases in U(VI) reduction rates may have also contributed to the observed rise in effluent U concentrations.

Uranium Aqueous Speciation. Although effluent U concentrations were relatively low (~1 μM), our cryogenic fluorescence spectra show good resolution (Figure 3). The uranyl fluorescence spectrum of the effluent sample collected before reduction occurred resembles that of $Ca_2UO_2(CO_3)_3$ (aq), while the spectrum from the reoxidation stage effluent is more similar to that of $(UO_2)(CO_3)_3^{4-}$ (*17*). Assuming that $Ca_2UO_2(CO_3)_3$ and $(UO_2)(CO_3)_3^{4-}$ are the only uranyl species present in the effluent samples, spectral deconvolution based on the normalized fluorescence spectra indicate that the earlier effluent sample is composed of nearly 100% ($Ca_2UO_2(CO_3)_3$, and the reoxidation stage effluent U is composed of 61% $(UO_2)(CO_3)_3^{4-}$ and 39% $Ca_2UO_2(CO_3)_3$. The fluorescence lifetime of the earlier effluent sample (1204 μs) is consistent with that of the $Ca_2UO_2(CO_3)_3$ complex (1282 μs), and that of the reoxidation stage effluent (1100 μs) falls between those of $(UO_2)(CO_3)_3^{4-}$ (883 μs) and $Ca_2UO_2(CO_3)_3$ (1282 μs). It should be noted that based on solution chemistry (Table 2), equilibrium calculations (MINEQ+, with updated constants provided in Supporting Information) predict that $Ca_2UO_2(CO_3)_3$, $(UO_2)(CO_3)_3^{4-}$, $(UO_2)(CO_3)_2^{2-}$, and $CaUO_2(CO_3)_3^{2-}$ should comprise 80.8%, 11.4%, 4.3%, and 3.6% of the aqueous U species, respectively. Although we do not have an explanation for differences between laser fluorescence spectra and model predictions, the results and spectra of other column effluents (not shown) are consistent in that

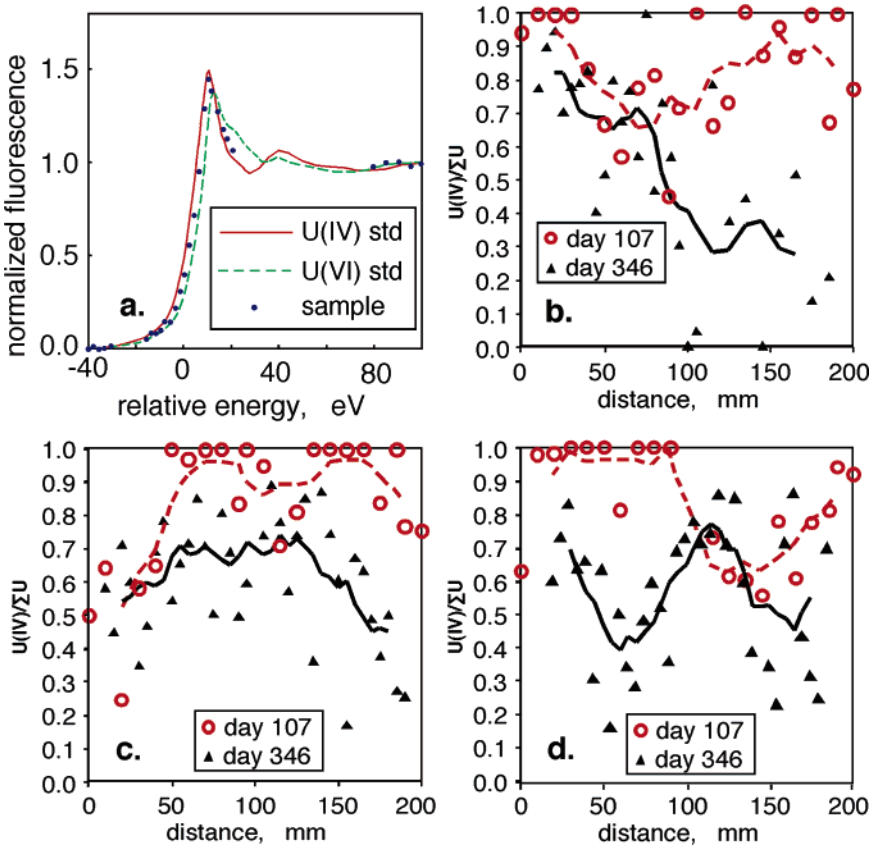

FIGURE 2. Micro-XANES spectra of U(IV) fractions in sediments. (a) Examples of XANES spectra from U(IV) and U(VI) standards, and from a location within a sediment column. (b−d) Profiles from three sediment columns obtained on days 107 and 346. Individual measurements are shown as points, while 5-point moving averages are shown as curves. Measurements within sediments on the two different days were not necessarily obtained at identical locations.

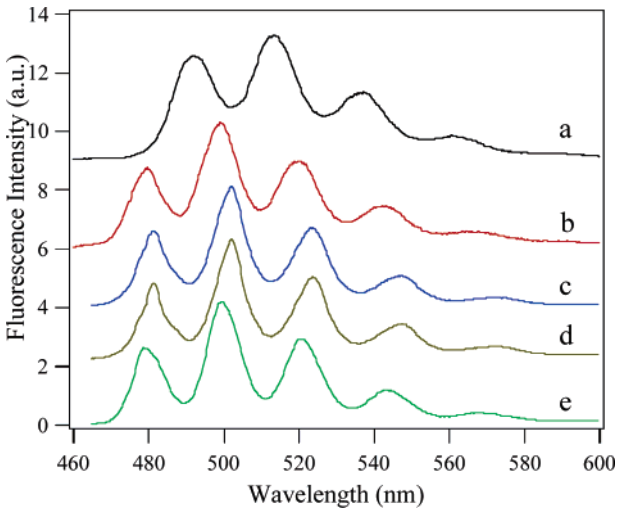

FIGURE 3. Fluorescence spectra of aqueous uranyl complexes at 6 K, with $\lambda_{ex} = 415$ nm. (a) Uranyl ion [UO_2^{2+}]; (b) $(UO_2)(CO_3)_3^{4-}$; (c) $Ca_2UO_2(CO_3)_3$; (d) effluent sample collected before reduction; (e) effluent sample collected during the steady-state reoxidation stage. Spectra are normalized to the same maximum intensities and offset along the vertical axis.

tricarbonate solution complexes (with and without Ca) are dominant.

Microbial Community. The continuing consumption of OC and efflux of respiration products (Figure 1b,c) indicated stable microbial activity through the reduction and reoxidation stages. Data from high-density oligonucleotide arrays indicated that functional groups of relevance within the microbial community remained stable as the 16S rDNA amplicon abundance of most *Geobacteraceae* detected did not change significantly ($p > 0.05$) between the reducing and oxidizing stages (Table 3). The fact that amplicon abundance of these OTUs did not vary with distance along columns demonstrates that an adequate supply of OC was reaching all sediment regions. Real-time PCR was used to quantify *Geobacteraceae* 16S rDNA gene copies in sediment extracts and confirmed array observations that the cell densities of organisms within the *Geobacteraceae* remained consistent between the reduction (1.8×10^8 copies (g sediment)$^{-1}$) and oxidation stages ($(1.2-2.6) \times 10^8$ copies (g sediment)$^{-1}$). These results suggest that a microbial community capable of continued U reduction remained through the reoxidation phase and that a loss of microbial functionality was not a factor in U(IV) reoxidation. A possible explanation for the observed coexistence of this stable microbial community and ~1 μM U(VI) concentrations was provided by E. Roden (personal communication). Under conditions of very low concentrations of available TEAs characteristic of this experiment, growth rates for dissimilatory metal reducing bacteria are not high enough to sustain U(VI) reduction. However, it is possible that the energy required for maintaining biomass in these populations could have been produced through syntrophic associations with methanogens (*26*, *27*). Investigation of this possibility was beyond the scope of the present study.

Mechanisms. Steady-state lactate consumption and CO_2 production as well as microarray-based and quantitative PCR analysis of relevant portions of the sediment microbial community indicate that the microbial community remained unchanged between the net U-reducing and the U-oxidizing stages. Therefore, primarily geochemical processes were evaluated for explaining the observed increases in aqueous U(VI) concentrations and reoxidation of U. Overviews of expected dominant U species under our experimental conditions can be obtained through Eh−pH diagrams. Others have found that newly reduced U(IV) is usually poorly crystallized, in the form of nanoparticles (*28*, *29*) or surface precipitates (*30*). Therefore, the impact of increased P_{CO_2} on U redox equilibrium was calculated using amorphous U(IV), UO_2(am), as the representative tetravalent solid phase (thermodynamic constants are provided in the Supporting Information). It is recognized that UO_2(am) is not thermo-

TABLE 3. Quantitative Real-Time PCR and 16S Microarray Analyses of *Geobacteraceae* Populations during Net Reduction and Net Reoxidation Phases

		reduction	oxidation (bottom)	oxidation (middle)	oxidation (top)
qPCR	*Geobacteraceae* 16S rRNA genes (10^8 copies g^{-1} sediment)	1.8 ± 0.43	2.6 ± 1.10	1.2 ± 0.08	1.2 ± 0.48
16 S microarray[a]	sequence detected				
	Pelobacter acetylenicus subgroup prokMSA 79502[b]	2034	1917	1869	2022
	Pelobacter acetylenicus subgroup prokMSA 78912	1961	1957	1924	1980
	Desulfuromonas acetoxidans subgroup prokMSA 76391	2839	2764	2836	2929
	Geobacter metallireducens subgroup prokMSA 60598	2102	1978	2076	2231
	Geobacter metallireducens subgroup prokMSA 10717[c]	942	771	781	802
	Geobacter metallireducens subgroup prokMSA 10726	2250	2214	2160	2224
	Geobacter metallireducens subgroup prokMSA 79548	1664	1327	1354	1535
	Geobacter metallireducens subgroup prokMSA 79712	2484	2364	2412	2722
	Geobacter metallireducens subgroup prokMSA 71753	3674	3145	3237	3340
	Geobacter metallireducens subgroup prokMSA 63255	2971	2997	2742	3028

[a] Values shown are the mean average difference (AD) for three replicates. [b] prokMSA numbers refer to the specific OTU detected using the 16S microarray − sequences are available online at http://greengenes.lbl.gov/jsp/search.jsp. [c] Only this OTU within the detected *Geobacteraceae* changed significantly ($p < 0.05$) between reduction and oxidation phases.

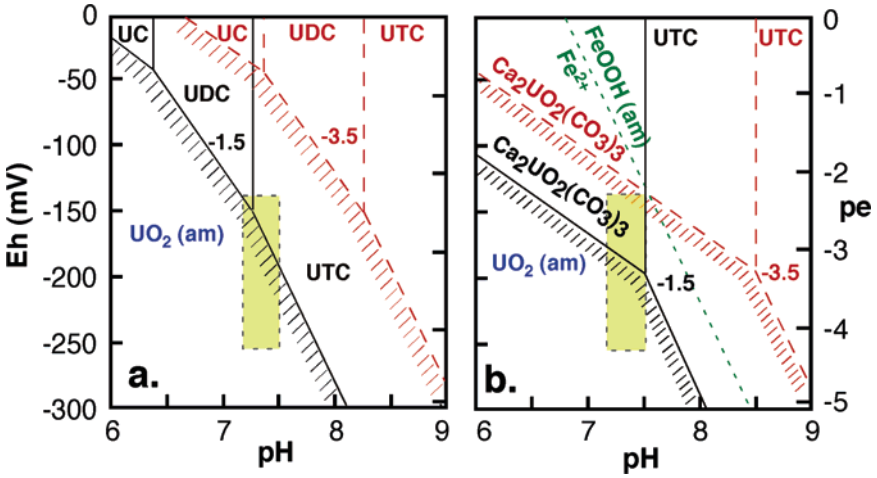

FIGURE 4. Stability regions for U species (a) without Ca^{2+}, and (b) with Ca^{2+} in equilibrium with calcite. UC, UDC, and UTC denote $UO_2CO_3^0$, $UO_2(CO_3)_2^{2-}$, and $UO_2(CO_3)_3^{4-}$, respectively. Total U(VI) = 10^{-6} M. Boundaries are shown for $PCO_2 = 10^{-1.5}$ atm (black) and $10^{-3.5}$ atm (red). The experimental conditions are within the Eh(pH) range indicated by the yellow rectangles. The Fe^{2+}/FeOOH(am) boundary (40 μM Fe^{2+}) is shown in panel b for comparison. It should be noted that the +calcite diagram (b) becomes less representative at pH < 7 because of unlikely equilibria requiring increasingly higher [Ca^{2+}].

dynamically well defined, but provides more realistic predictions of solubilities over shorter time scales following reduction. This sediment contained 3% $CaCO_3$, and the influent solution contained 1 mM Ca^{2+}, so that the $Ca_2UO_2(CO_3)_3$ aqueous complex (*16*) could be important. In view of uncertainties associated with the $Ca_2UO_2(CO_3)_3$ stability constant (*31*), our calculations related to this species are provisional. Complexes of UO_2^{2+} with lactate and acetate are insignificant in carbonate-rich, neutral waters such as those of our column effluents, based on comparisons of stability constants for carbonato (*16*, *31*), lactate (*32*), and acetate (*33*) complexes. U(VI)/U(IV) equilibrium shifts toward lower redox potentials when P_{CO_2} increases from $10^{-3.5}$ to $10^{-1.0}$ atm (other conditions constant), as shown in Figure 4. The presence of Ca^{2+} is also predicted to enhance U solubility at low pe through formation of $Ca_2UO_2(CO_3)_3$(aq). Included in these diagrams is the pe(pH) region characteristic of the sediment columns, showing that the reducing experimental conditions can shift equilibria toward U(VI) in response to increased P_{CO_2}. Thus, oxidation of previously precipitated UO_2(am) and increased aqueous U(VI) concentrations are thermodynamically favored if residual TEAs are available under elevated P_{CO_2} condition. The fact that net reoxidation of U was directly measured indicates that a suitable TEA was still present.

Several lines of evidence suggest that the likely TEA(s) in these sediment columns are Fe(III) and possibly Mn(IV) oxides. First, poorly crystalline Fe(III) oxyhydroxide and MnO_2 are common in sediments. This Oak Ridge sediment contains 4.4% (790 mmol kg^{-1}) Fe, with 65.7 mmol kg^{-1} originally in weak acid extractable form (*34*), and with the reactive citrate-dithionite extractable Fe (*35*) remaining at the end of this experiment ranging from 340 to 480 mmol kg^{-1}. An important difference between our column experiments and studies based on well-stirred suspensions is that the vigorous mixing employed in the latter allows for much more uniform changes toward equilibrium, such that Fe(III) and Mn(IV) oxides would expect to be depleted (reduced) at the completion of U reduction. However, even in such well-mixed suspensions, Fe(III) and Mn(IV) oxides have been found under anaerobic conditions upon completion of U reduction (*28*, *36*, *37*), indicating that they could easily persist for hundreds of days in columns (and in nature) where mixing is much weaker and where solid/water ratios are high. Second, the measured steady-state Fe^{2+} and Mn^{2+} concentrations in the effluent solutions (42 and 35 μM, respectively) are supersaturated with respect to siderite and rhodochrosite, respectively, and substantially greater than effluent U(VI) concentrations (1 μM). Third, the ability of sediment Fe(III) and Mn(IV) oxides to oxidize U(IV) in the presence of electron shuttles has been shown (*28*, *36*, *37*), and soluble Fe(III) has been reported in the pore waters of reduced sedimentary material containing crystalline and/or amorphous Fe-oxides (*38*). Finally, the other potential TEAs, O_2, NO_3^-(NO_2^-), and SO_4^{2-}, were undetectable in column solutions. A hypothesis to be tested in future work is that kinetic limitations allow very low concentrations of reactive Fe(III) and possibly Mn(IV) oxides to serve as TEAs under sustained reducing conditions.

Although the factors just discussed indicate that Fe(III) oxides may serve as TEAs for the observed U(IV) oxidation, the thermodynamic drive for this reaction is highly sensitive to the solid phases involved, concentrations of aqueous species, and pH. For example, if $Ca_2UO_2(CO_3)_3$ is the dominant U(VI) species, the reaction

$$UO_2(am) + 2FeOOH(s) + 3HCO_3^- + 2Ca^{2+} + 3H^+ = Ca_2UO_2(CO_3)_3 + 2Fe^{2+} + 4H_2O \quad (1)$$

under conditions specified for effluents in Table 2 has a ΔG of +23.8 kJ mol^{-1} for goethite (α-FeOOH), and −29.4 kJ mol^{-1} for amorphous FeOOH (thermodynamic constants provided in the Supporting Information). Similarly, with $UO_2(CO_3)_3^{4-}$ as the dominant U(VI) species, the reaction

$$UO_2(am) + 2FeOOH(s) + 3HCO_3^- + 3H^+ = UO_2(CO_3)_3^{4-} + 2Fe^{2+} + 4H_2O \quad (2)$$

has a ΔG of +41.3 kJ mol^{-1} for α-FeOOH, and −11.9 kJ mol^{-1} for amorphous FeOOH. The related problem concerning the highly variable effectiveness of abiotic U(VI) reduction by Fe(II) in the presence of different Fe(III) oxides has been addressed recently by Jeon et al. (*35*).

While these considerations point to Fe(III) and possibly Mn(IV) oxides as the most likely TEAs, it is also important to recognize that only very small concentrations of these postulated oxidants are required. Our measured change in the U(IV) fraction of this heavily contaminated sediment, from 0.87 to 0.58, amounts to reoxidizing 0.25 mmol U (kg sediment)$^{-1}$, which would have only required 0.50 mmol (kg sediment)$^{-1}$ of reactive Fe(III).

Summary and Implications for in-Situ U Remediation. This paper presents evidence that bioreduced U(IV) is reoxidized under reducing conditions because carbonate accumulation promotes the formation of highly stable carbonato−U(VI) complexes under neutral to slightly alkaline conditions. The results presented here are useful for understanding and designing OC-based treatment of field sediments because the experiment was conducted on historically U contaminated sediment supplied with lactate-enriched simulated groundwater, at reasonable groundwater flow-rates, with most measurements obtained via noninvasive techniques. Our results show that OC concentrations in remedial solutions need to be carefully considered to minimize carbonate-enhancement of U(VI) solubilities. Impacts of carbonato−U(VI) species are diminished in acidic sediments where these complexes become insignificant, and when carbonate concentrations are kept low. Although the effects of pH, pe, CO_2, and Ca^{2+} on U(VI) equilibrium are established (*2*, *16*, *31*), their implications on OC-based, reductive U stabilization have not previously been appreciated. This work also demonstrates the need for long-term experiments for evaluating remediation strategies that rely on transforming actinides and metals to low solubility products. Even when U bioreduction is successful, maintenance of reduction-based treatments may be impractical within regionally oxidizing sediments, given the very long time scales set by the 4.5×10^9 year half-life of ^{238}U.

Acknowledgments

We thank E. Roden, W. Lukens, S. Traina, G. Sposito, the anonymous reviewers, and Associate Editor J. Hering for helpful review comments. Experimental support by J. Larsen, D. Joyner, S. Baek, J. Pena, and M. Newville is gratefully acknowledged. We thank D. Watson for providing Oak Ridge FRC field sediment samples, G. Anderson and T. DeSantis for providing microarray facilities and expertise, and J. Coates for generously donating *Geobacter metallireducens* GS-15 cells. Funding was provided by the U.S. Department of Energy (DOE), NABIR Program, the Basic Energy Sciences (BES) Geosciences Program, GeoSoilEnviroCARS (GSECARS), Advanced Photon Source (APS), Argonne National Laboratory. GSECARS is supported by the National Science Foundation − Earth Sciences, DOE − Geosciences, and the State of Illinois. Use of the APS was supported by the DOE BES, Office of Energy Research. Fluorescence spectroscopic measurements were performed at the W.R. Wiley Environmental Molecular Sciences Laboratory, a national scientific user facility sponsored by the DOE's Office of Biological and Environmental Research.

Supporting Information Available

Thermodynamic constants. This material is available free of charge via the Internet at http://pubs.acs.org.

Literature Cited

(1) U.S. Department of Energy. Status Report on Paths to Closure. http://web.em.doe.gov/closure/fy2000/index.html. U.S. Department of Energy: Washington, DC, 2002.
(2) Langmuir, D. *Aqueous Environmental Geochemistry*; Prentice Hall: Upper Saddle River, NJ, 1997.
(3) Lovley, D. R.; Phillips, E. J. P.; Gorby, Y. A.; Landa, E. R. Microbial reduction of uranium. *Nature* **1991**, *350*, 413−416.
(4) Lovley, D. R.; Roden, E. E.; Phillips, E. J. P.; Woodward, J. C. Enzymatic iron and uranium reduction by sulfate-reducing bacteria. *Mar. Geol.* **1993**, *113*, 41−53.
(5) Ganesh, R.; Robinson, K. G.; Reed, G. D.; Sayler, G. S. Reduction of hexavalent uranium from organic complexes by sulfate- and iron-reducing bacteria. *Appl. Environ. Microbiol.* **1997**, *63*, 4385−4391.
(6) Fredrickson, J. K.; Zachara, J. M.; Kennedy, D. W.; Duff, M. C.; Gorby, Y. A.; Li, S. W.; Krupka, K. M. Reduction of U(VI) in goethite (α-FeOOH) suspensions by a dissimilatory metal-reducing bacterium. *Geochim. Cosmochim. Acta* **2000**, *64*, 3085−3098.
(7) Uhrie, J. L.; Drever, J. I.; Colberg, P. J. S.; Nesbitt, C. C. In situ immobilization of heavy metals associated with uranium leach mines by bacterial sulfate reduction. *Hydrometallurgy* **1996**, *43*, 231−239.
(8) Abdelouas, A.; Lu, Y.; Lutze, W.; Nuttall, H. E. Reduction of U(VI) to U(IV) by indigenous bacteria in contaminated ground water. *J. Contam. Hydrol.* **1998**, *35*, 217−233.
(9) Anderson, R. T.; Vrionis, H. A.; Ortiz-Bernad, I.; Resch, C. T.; Long, P. E.; Dayvault, R.; Karp, K.; Marutzky, S.; Metzler, D. R.; Peacock, A.; White, D. C.; Lowe, M.; Lovley, D. R. Stimulating the in situ activity of Geobacter species to remove uranium from the groundwater of a uranium-contaminated aquifer. *Appl. Environ. Microbiol.* **2003**, *69*, 5884−5891.
(10) Casas, I.; Gimenez, J.; Marti, V.; Torrero, M. E.; de Pablo, J. Kinetic studies of unirradiated UO_2 dissolution under oxidizing conditions in batch and flow experiments. *Radiochim. Acta* **1994**, *66/67*, 23−27.
(11) Finneran, K. T.; Housewright, M. E.; Lovley, D. R. Multiple influences of nitrate on uranium solubility during bioremediation of uranium-contaminated subsurface sediments. *Environ. Microbiol.* **2002**, *4*, 510−516.
(12) Senko, J. M.; Istok, J. D.; Suflita, J. M.; Krumholz, L. R. In-situ evidence for uranium immobilization and remobilization. *Environ. Sci. Technol.* **2002**, *36*, 1491−1496.
(13) U.S. Department of Energy's Natural and Accelerated Bioremediation Research (NABIR) Program's Field Research Center, http://public.ornl.gov/nabirfrc/, 2003.
(14) Bertsch, P. M.; Hunter, D. B. Applications of synchrotron-based X-ray microprobes. *Chem. Rev.* **2001**, *101*, 1809−1842.
(15) Duff, M. C.; Morris, D. E.; Hunter, D. B.; Bertsch, P. M. Spectroscopic characterization of uranium in evaporation basin sediments. *Geochim. Cosmochim. Acta* **2000**, *64*, 1535−1550.
(16) Bernhard, G.; Geipel, G.; Reich, T.; Brendler, V.; Amayri, S.; Nitsche, H. Uranyl(VI) carbonate complex formation: Validation of the Ca2UO2(CO3)(3)(aq.) species. *Radiochim. Acta* **2001**, *89*, 511−518.
(17) Wang, Z.; Zachara, J. M.; Yantanssee, W.; Liu, C.; Gassman, P. L.; Joly, A. G. Cryogenic laser induced fluorescence characterization of U(VI) in Hanford vadose zone pore waters. *Environ. Sci. Technol.* **2004**, *38*, 5591−5597.
(18) Wilson, K. H.; Blitchington, R. B.; Greene, R. C. Amplification of bacterial 16S ribosomal DNA with polymerase chain reaction. *J. Clin. Microbiol.* **1990**, *28*, 1942−1946.
(19) DeSantis, T. Z.; Dubosarskiy, I.; Murray, S. R.; Andersen, G. L. Comprehensive aligned sequence construction for automated design of effective probes (CASCADE-P) using 16S rDNA. *Bioinformatics* **2003**, *19*, 1461−1468.
(20) Masuda, N.; Church, G. M. *Escherichia coli* gene expression responsive to levels of the response regulator EvgA. *J. Bacteriol.* **2002**, *184*, 6225−6234.
(21) Holmes, D. E.; Finneran, K. T.; O'Neil, R. A.; Lovley, D. R. Enrichment of members of the family *Geobacteraceae* associated with stimulation of dissimilatory metal reduction in uranium-contaminated aquifer sediments. *Appl. Environ. Microbiol.* **2002**, *68*, 2300−2306.
(22) U.S. Environmental Protection Agency's Maximum Contaminant Level for U, amendment to 40 CFR Part 141 (65 FR 76708, Dec. 7, 2000).
(23) Missana, T.; Garcia-Gutierrez, M.; Alonso, U. Kinetics and irreversibility of cesium and uranium sorption onto bentonite colloids in a deep granitic environment. *Appl. Clay Sci.* **2004**, *26*, 137−150.
(24) Jeon, B. H.; Kelly, S. D.; Kemner, K. M.; Barnett, M. O.; Burgos, W. D.; Dempsey, B. A.; Roden, E. E. Microbial reduction of U(VI) at the solid-water interface. *Environ. Sci. Technol.* **2004**, *38*, 5649−5655.
(25) Ortiz-Bernad, I.; Anderson, R. T.; Vrionis, H. A.; Lovley, D. R. Resistance of solid-phase U(VI) to microbial reduction during in situ bioremediation of uranium-contaminated groundwater. *Appl. Environ. Microbiol.* **2004**, *70*, 7558−7560.
(26) Schink, B. Energetics of syntrophic cooperation in methanogenic degradation. *Microbiol. Mol. Biol. Rev.* **1997**, *61*, 262−280.
(27) Cord-Ruwisch, R.; Lovley, D. R.; Schink, B. Growth of *Geobacter sulfurreducens* with acetate in syntrophic cooperation with hydrogen-oxidizing anaerobic partners. *Appl. Environ. Microbiol.* **1998**, *64*, 2232−2236.
(28) Fredrickson, J. K.; Zachara, J. M.; Kennedy, D. W.; Liu, C.; Duff, M. C.; Hunter, D. B.; Dohnalkova, A. Influence of Mn oxides on

the reduction of uranium (VI) by the metal-reducing bacterium Shewanella putrefaciens. *Geochim. Cosmochim. Acta* **2002**, *66*, 3247−3262.
(29) Suzuki, Y.; Kelly, S. D.; Kemner, K. M.; Banfield, J. F. Nanometre-size products of uranium bioreduction. *Nature* **2002**, *419*, 134.
(30) Giammar, D. E.; Hering, J. G. Time scales for sorption−desorption and surface precipitation of uranyl on goethite. *Environ. Sci. Technol.* **2001**, *35*, 3332−3337.
(31) Guillaumont, R.; Fanghanel, T.; Fugen, J.; Grenthe, I.; Neck, V.; Palmer, D. A.; Rand, M. H. *Chemical Thermodynamics 5. Update on the Chemical Thermodynamics of Uranium, Neptunium, Plutonium, Americium, and Technetium*; Nuclear Energy Agency; Elsevier: Amsterdam, 2003.
(32) Portanova, R.; Lajunen, L. H. J.; Tolazzi, M.; Piispanen, J. Critical evaluation of stability constants for a-hydroxycarboxylic acid complexes with protons and metal ions and the accompanying enthalpy changes, Part II. Aliphatic 2-hydroxycarboxylic acids. *Pure Appl. Chem.* **2003**, *75*, 495−540.
(33) Jiang, J.; Rao, L.; Di Bernardo, P.; Zanonato, P. L.; Bismondo, A. Complexation of uranium(VI) with acetate at variable temperatures. *J. Chem. Soc., Dalton Trans.* **2002**, *2002*, 1832−1838.
(34) Zheng, Z.; Wan, J. Release of contaminant U(VI) from soils. *Radiochim. Acta* **2005**, *93*, 211−217.
(35) Jeon, B. H.; Dempsey, B. A.; Burgos, W. D.; Barnett, M. O.; Roden, E. E. Chemical reduction of U(VI) by Fe(II) at solid-water interface using natural and synthetic Fe(III) oxides. *Environ. Sci. Technol.*, accepted for publication.
(36) Fredrickson, J. K.; Zachara, J. M.; Kennedy, D. W.; Duff, M. C.; Gorby, Y. A.; Li, S. w.; Krupka, K. M. Reduction of U(VI) in goethite (α-FeOOH) suspensions by a dissimilatory metal-reducing bacterium. *Geochim. Cosmochim. Acta* **2000**, *64*, 3085−3098.
(37) Nevin, K. P.; Lovley, D. R. Potential for nonenzymatic reduction of Fe(III) via electron shuttling in subsurface sediments. *Environ. Sci. Technol.* **2000**, *34*, 2472−2478.
(38) Nevin, K. P.; Lovley, D. R. Mechanisms for Fe(III) oxide reduction in sedimentary environments. *Geomicrobiol. J.* **2002**, *19*, 141−159.

Received for review November 11, 2004. Revised manuscript received June 17, 2005. Accepted June 17, 2005.

ES048236G